Mechanical Systems and Signal Processing 129 (2019) 218–234

Contents lists available at ScienceDirect

Mechanical Systems and Signal Processing

journal homepage: www.elsevier.com/locate/ymssp

A dynamic condensation method with free interface substructuring

Jeong-Ho Kim [a,b], Seung-Hwan Boo [c], Phill-Seung Lee [a,*]

[a] Department of Mechanical Engineering, Korea Advanced Institute of Science and Technology, 291 Daehak-ro, Yuseong-gu, Daejeon 34141, Republic of Korea
[b] Korea Institute of Nuclear Safety, 62 Gwahak-ro, Yuseong-gu, Daejeon 34142, Republic of Korea
[c] Division of Naval Architecture and Ocean Systems Engineering, Korea Maritime and Ocean University, 727 Taejong-ro, Yeongdo-gu, Busan, Republic of Korea

ARTICLE INFO

Article history:
Received 18 April 2018
Received in revised form 30 January 2019
Accepted 12 April 2019

Keywords:
Structural dynamics
Finite element method
Model reduction
Improved reduced system method
Substructuring
Free interface

ABSTRACT

In this paper, a novel dynamic condensation method is proposed with free interface substructuring, in which the substructures are completely decoupled. The substructures are independently defined and the substructural finite element (FE) models are individually reduced by adopting the improved reduced system (IRS) method. The reduced mass and stiffness matrices of substructures are assembled using a Lagrange multiplier vector, leading to the final reduced model. Using the proposed method, each of the substructural FE models can be reduced in parallel without coupling among the neighboring substructures. Thus, the method can be applied with ease to substructures connected through non-matching meshes. Moreover, complicated substructural interfaces can be accommodated when employing this method. The formulation of the proposed method is presented in detail, and its accuracy, computational efficiency, and modeling ability are investigated using several demonstrative engineering problems.

1. Introduction

For several decades, dynamic condensation [1–9] and component mode synthesis (CMS) [10–25] methods have been widely used to obtain reduced models in many engineering fields. The distinct difference between those methods is that, while dynamic condensations [1–9] provide reduced models in physical coordinates, CMS methods [10–25] provide those in modal (non-physical) coordinates. Due to this fact, the methods have been utilized in different applications. In particular, dynamic condensations are specialized for experimental-finite element (FE) model correlation, sensor positioning, and FE model updating [6–9].

In automobile, aerospace, and shipbuilding industries, structures are constructed by combining many small and large substructures (component structures). The substructures are individually designed, manufactured, and tested by different development groups. For analyzing an entire structure, it is beneficial to construct a finite element (FE) model of the structure by integrating the substructural FE models already built by each development group. This is especially useful, when frequent design modifications are necessary for individual substructures. Such substructuring is a key feature of the CMS methods [10–25]. However, the original dynamic condensation methods [1–9] do not offer these advantageous features of substructuring. It is also difficult to handle the FE models with large degrees of freedom (DOF) using the methods.

* Corresponding author.
E-mail address: phillseung@kaist.edu (P.-S. Lee).

https://doi.org/10.1016/j.ymssp.2019.04.021
0888-3270/

Bouhaddi and Fillod applied substructuring to Guyan reduction [26,27]. Cho et al. applied physical domain-based substructuring to the improved reduced system (IRS) and the iterative IRS methods, and employed a penalty frame method for considering non-matched subdomains [28–31]. These substructuring algorithms were based on a fixed interface boundary. The substructures were coupled through a unique set of physical interface DOFs. While the algorithms are simple and robust, a fully coupled FE model is required in advance to obtain a reduced model [26–33].

In this study, we focus on developing a dynamic condensation method with free interface substructuring, in which the substructural FE models employ a fully decoupled computation. The new method provides several advantages owing to the free interface substructuring [19–23]. Complicated physical interfaces and non-matching meshes among the substructures can be handled easily. Individual substructural FE models are independently defined using the substructural equations of motion and compatibility conditions with a free interface boundary. Then, the substructural models are reduced by adopting the IRS method [2]. The reduced mass and stiffness matrices are obtained through a simple assembly of reduced substructural matrices.

The two novel features of the proposed method are as follows: first, the complete independence of each substructural FE model is maintained during the reduction process. A local change in a substructural FE model does not require an update of the entire reduced model and thus, the method is effective, when frequent reanalysis is required due to design modifications. Second, the method can handle relatively large and complex FE models compared to Guyan reduction [1] and the IRS methods [2]. Complicated substructural interfaces (e.g., hinge, slip, contact, etc.) and substructures with non-matching meshes can be modeled using this method.

In Section 2, we briefly review the IRS method [2]. In Section 3, the substructuring algorithm with free interface is introduced and the formulation and reduction procedures of the proposed method are described. In Section 4, the performance and the modeling ability of the proposed method is presented using various numerical examples. Finally, the conclusions are presented in Section 5.

2. Improved reduced system (IRS) method

In this section, we briefly introduce the formulation of the improved reduced system (IRS) method, see Ref. [2] for detailed derivations.

In the IRS method, the equations of motion for undamped free vibration are given by

$$\mathbf{M}_g\ddot{\mathbf{U}}_g + \mathbf{K}_g\mathbf{U}_g = \mathbf{0} \quad \text{with} \quad \mathbf{M}_g = \begin{bmatrix} \mathbf{M}_{ss} & \mathbf{M}_{sm} \\ \mathbf{M}_{ms} & \mathbf{M}_{mm} \end{bmatrix}, \mathbf{K}_g = \begin{bmatrix} \mathbf{K}_{ss} & \mathbf{K}_{sm} \\ \mathbf{K}_{ms} & \mathbf{K}_{mm} \end{bmatrix}, \mathbf{U}_g = \begin{bmatrix} \mathbf{U}_s \\ \mathbf{U}_m \end{bmatrix}, \tag{1}$$

in which $\mathbf{M}_g$ and $\mathbf{K}_g$ are the mass and stiffness matrices for the global (original) FE model (see Fig. 1a), and $\mathbf{U}_g$ is the corresponding displacement vector. The subscripts s and m denote the 'slave' and 'master' DOFs, respectively (see Fig. 1b). Note that $(\ddot{\ }) = \mathrm{d}^2(\ )/\mathrm{d}t^2$ with time variable t.

Considering the harmonic response $\mathbf{U}_g = \mathbf{u}_g e^{i\omega t}$ in Eq. (1), the original eigenvalue problem can be indicated by

$$\begin{bmatrix} \mathbf{K}_{ss} & \mathbf{K}_{sm} \\ \mathbf{K}_{ms} & \mathbf{K}_{mm} \end{bmatrix} \begin{bmatrix} \mathbf{u}_s \\ \mathbf{u}_m \end{bmatrix} = \lambda \begin{bmatrix} \mathbf{M}_{ss} & \mathbf{M}_{sm} \\ \mathbf{M}_{ms} & \mathbf{M}_{mm} \end{bmatrix} \begin{bmatrix} \mathbf{u}_s \\ \mathbf{u}_m \end{bmatrix} \text{with} \, \mathbf{u}_g = \begin{bmatrix} \mathbf{u}_s \\ \mathbf{u}_m \end{bmatrix}, \tag{2}$$

where λ and $\mathbf{u}_g$ are the eigenvalue ($\lambda = \omega^2$) and eigenvector of the global FE model, and $\mathbf{u}_s$ and $\mathbf{u}_m$ are the eigenvectors corresponding to the slave and master DOFs ($\mathbf{U}_s$ and $\mathbf{U}_m$), respectively. From the first row in Eq. (2), $\mathbf{u}_s$ is represented by

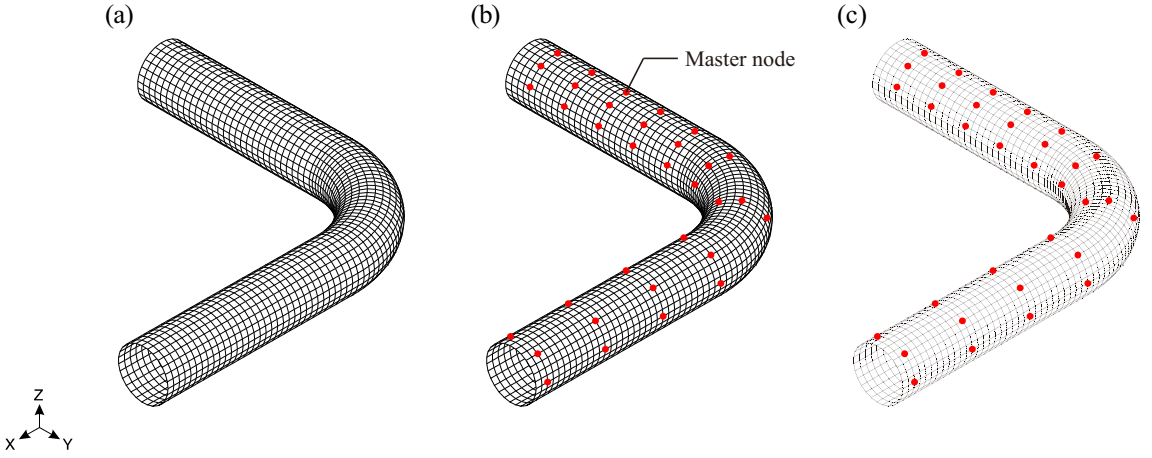

Fig. 1. Reduction procedure of the IRS method: (a) Original FE model, (b) Selection of master nodes (The remaining unselected nodes are slave nodes.), (c) Reduced model.

$$\mathbf{u}_s = -(\mathbf{K}_{ss} - \lambda\mathbf{M}_{ss})^{-1}(\mathbf{K}_{sm} - \lambda\mathbf{M}_{sm})\mathbf{u}_m. \tag{3}$$

Using the Neumann series expansion [13–20], Eq. (3) can be expanded

$$\mathbf{u}_s = -(\mathbf{K}_{ss}^{-1} + \lambda\mathbf{K}_{ss}^{-1}\mathbf{M}_{ss}\mathbf{K}_{ss}^{-1} + o(\lambda^2) + o(\lambda^3) + \cdots)(\mathbf{K}_{sm} - \lambda\mathbf{M}_{sm})\mathbf{u}_m, \tag{4}$$

and neglecting terms higher than the order of λ, $\mathbf{u}_s$ is approximated as follows

$$\mathbf{u}_s \approx \bar{\mathbf{u}}_s = [-\mathbf{K}_{ss}^{-1}\mathbf{K}_{sm} + \lambda\mathbf{K}_{ss}^{-1}(\mathbf{M}_{sm} - \mathbf{M}_{ss}\mathbf{K}_{ss}^{-1}\mathbf{K}_{sm})]\,\mathbf{u}_m. \tag{5}$$

Then, the global eigenvector $\mathbf{u}_g$ can be approximated as

$$\mathbf{u}_g \approx \bar{\mathbf{u}}_g = \begin{bmatrix} \bar{\mathbf{u}}_s \\ \mathbf{u}_m \end{bmatrix} = (\mathbf{T}_0 + \lambda\mathbf{T}_a)\mathbf{u}_m, \tag{6a}$$

$$\text{with}\,\mathbf{T}_0 = \begin{bmatrix} -\mathbf{K}_{ss}^{-1}\mathbf{K}_{sm} \\ \mathbf{I}_m \end{bmatrix},\ \mathbf{T}_a = \begin{bmatrix} \mathbf{K}_{ss}^{-1}(\mathbf{M}_{sm} - \mathbf{M}_{ss}\mathbf{K}_{ss}^{-1}\mathbf{K}_{sm}) \\ \mathbf{0} \end{bmatrix}, \tag{6b}$$

where $\mathbf{T}_0$ is called the Guyan transformation matrix [1], $\mathbf{T}_a$ is the additional transformation matrix containing the inertial effect of the slave DOFs, and $\mathbf{I}_m$ is the identity matrix corresponding to the master DOFs.

In the Guyan reduction, the approximated global eigenvector $\bar{\mathbf{u}}_g$ is simply defined by

$$\bar{\mathbf{u}}_g = \mathbf{T}_0\mathbf{u}_m, \tag{7}$$

and then, the reduced eigenvalue problem is obtained by

$$\bar{\mathbf{K}}_0\mathbf{u}_m = \bar{\lambda}\,\bar{\mathbf{M}}_0\mathbf{u}_m \text{ with } \bar{\mathbf{M}}_0 = \mathbf{T}_0^T\mathbf{M}_g\mathbf{T}_0,\ \bar{\mathbf{K}}_0 = \mathbf{T}_0^T\mathbf{K}_g\mathbf{T}_0, \tag{8}$$

in which $\bar{\mathbf{M}}_0$ and $\bar{\mathbf{K}}_0$ are the reduced mass and stiffness matrices, and $\bar{\lambda}$ is the approximated eigenvalue in the Guyan reduction.

Multiplying $\bar{\mathbf{M}}_0^{-1}$ on the both sides of Eq. (8), the following relation is obtained

$$\bar{\lambda}\,\mathbf{u}_m = \mathbf{H}_0\mathbf{u}_m \text{ with } \mathbf{H}_0 = \bar{\mathbf{M}}_0^{-1}\bar{\mathbf{K}}_0. \tag{9}$$

In Eq. (6a), using $\bar{\lambda}$ instead of λ, and applying the relation $\bar{\lambda}\,\mathbf{u}_m = \mathbf{H}_0\mathbf{u}_m$ in Eq. (9), the approximated global eigenvector $\bar{\mathbf{u}}_g$ can be more accurately defined as follows

$$\bar{\mathbf{u}}_g = \mathbf{T}_1\mathbf{u}_m \text{ with } \mathbf{T}_1 = \mathbf{T}_0 + \mathbf{T}_a\mathbf{H}_0, \tag{10}$$

where $\mathbf{T}_1$ is the transformation matrix of the IRS method [2].

Using the transformation matrix in Eq. (10), the reduced mass and stiffness matrices in the IRS method (see Fig. 1c) are calculated as

$$\bar{\mathbf{M}}_1 = \mathbf{T}_1^T\mathbf{M}_g\mathbf{T}_1 = \bar{\mathbf{M}}_0 + \mathbf{T}_0^T\mathbf{M}_g\mathbf{T}_a\mathbf{H}_0 + \mathbf{H}_0^T\mathbf{T}_a^T\mathbf{M}_g\mathbf{T}_0 + \mathbf{H}_0^T\mathbf{T}_a^T\mathbf{M}_g\mathbf{T}_a\mathbf{H}_0, \tag{11a}$$

$$\bar{\mathbf{K}}_1 = \mathbf{T}_1^T\mathbf{K}_g\mathbf{T}_1 = \bar{\mathbf{K}}_0 + \mathbf{T}_0^T\mathbf{K}_g\mathbf{T}_a\mathbf{H}_0 + \mathbf{H}_0^T\mathbf{T}_a^T\mathbf{K}_g\mathbf{T}_0 + \mathbf{H}_0^T\mathbf{T}_a^T\mathbf{K}_g\mathbf{T}_a\mathbf{H}_0. \tag{11b}$$

Finally, the reduced eigenvalue problem in the IRS method is given by

$$\bar{\mathbf{K}}_1(\bar{\boldsymbol{\varphi}}_1)_i = (\bar{\lambda}_1)_i\bar{\mathbf{M}}_1(\bar{\boldsymbol{\varphi}}_1)_i \ \text{ for } i = 1, 2, \cdots, N_m, \tag{12}$$

where $(\bar{\lambda}_1)_i$ and $(\bar{\boldsymbol{\varphi}}_1)_i$ are the approximated i^{th} eigenvalues and the corresponding eigenvectors, and N_m is the number of master DOFs, which determines the size of the reduced model.

In the IRS method, the global structural FE model is considered without substructuring. However, for a large FE model, the construction of $\mathbf{T}_1$ in Eq. (10) is computationally heavy or even impossible in a personal computer, because it contains expensive computations such as inversion of the large submatrix, $\mathbf{K}_{ss}^{-1}$ in Eq. (6). Boo and Lee overcame this issue in the algebraic dynamic condensation (ADC) method [32,33].

3. A new dynamic condensation method

In this section, we derive the formulation of a new dynamic condensation method with free interface substructuring. A free interface substructuring is performed, and each substructure is independently reduced by employing the IRS method. The reduced model is obtained by assembly of the substructural matrices calculated.

3.1. Free interface substructuring

In the proposed method, the global FE model is constructed of the N_s substructures assembled, which are interconnected through a free interface boundary Γ, using the compatibility between the interconnecting force and interface displacement, see Fig. 2.

In free interface substructuring [19–23], the linear dynamic equations for each substructure can be individually expressed by

$$\mathbf{M}^{(k)}\ddot{\mathbf{U}}^{(k)} + \mathbf{K}^{(k)}\mathbf{U}^{(k)} + \mathbf{B}^{(k)}\boldsymbol{\gamma} = \mathbf{f}^{(k)} \quad \text{for } k = 1, \cdots, N_s, \tag{13}$$

where $\mathbf{M}^{(k)}$ and $\mathbf{K}^{(k)}$ denote the mass and stiffness matrices of the k^{th} substructure, $\mathbf{U}^{(k)}$ is the corresponding displacement vector, and $\mathbf{f}^{(k)}$ is the external load vector applied to the substructure. To satisfy the force equilibrium in the assembly, $\mathbf{B}^{(k)}\boldsymbol{\gamma}$ is applied as the interconnecting force between substructures with Boolean matrix $\mathbf{B}^{(k)} = \begin{bmatrix} \mathbf{0} \\ \mathbf{b}^{(k)} \end{bmatrix}$ and the Lagrange multiplier vector $\boldsymbol{\gamma}$. Note that, unlike the previous studies [19–22], we express the Boolean matrix as $\mathbf{B}$ instead of $\mathbf{B}^T$.

To satisfy the displacement compatibility, the following constraint equation is explicitly enforced [19–23].

$$\sum_{k=1}^{N_s} \mathbf{b}^{(k)^T} \mathbf{U}_b^{(k)} = \mathbf{0}, \tag{14}$$

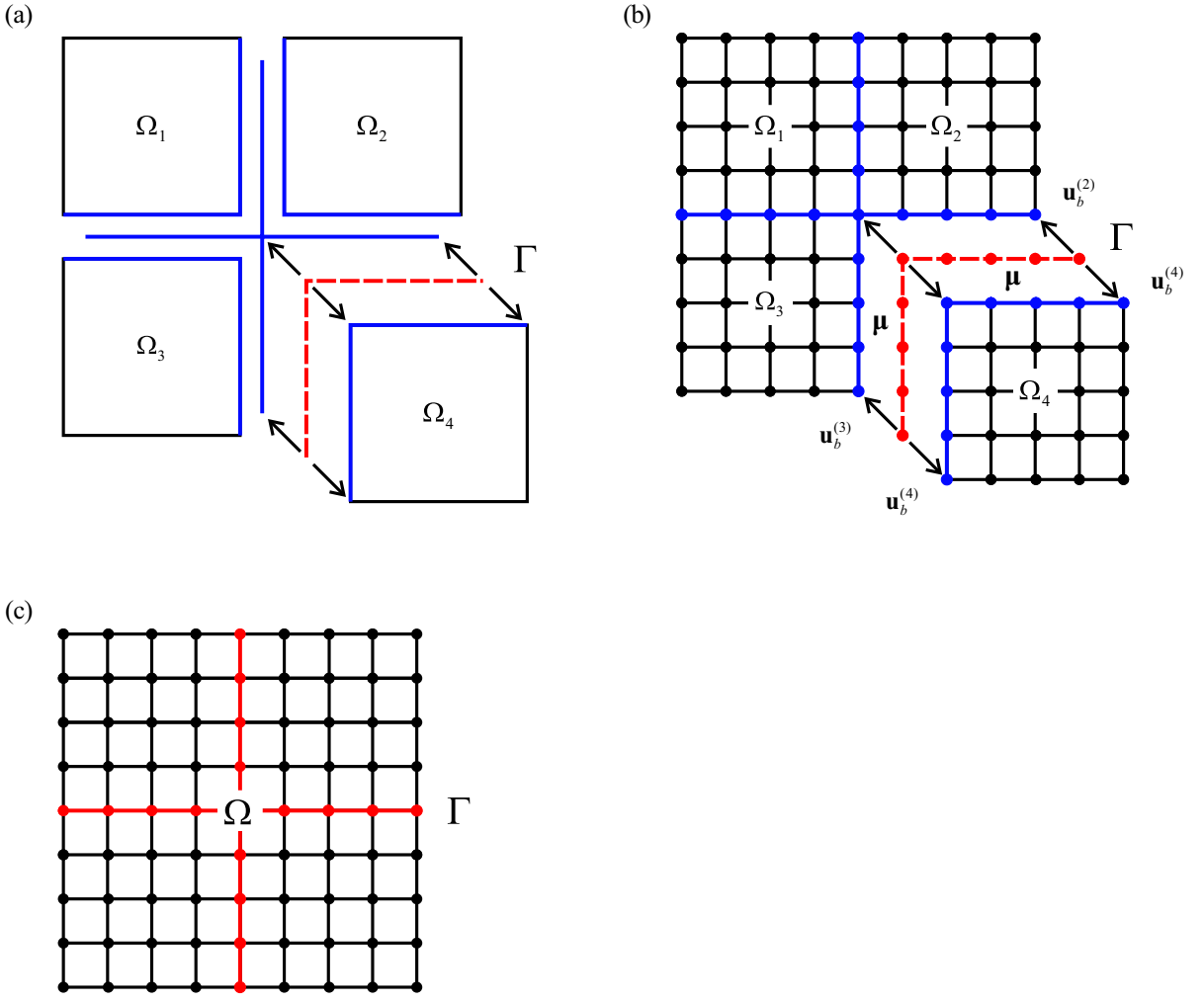

Fig. 2. Assemblage of substructures and interface handling in the proposed method ($N_s = 4$) [23]: (a) Substructures, Ω_1, Ω_2, Ω_3, and Ω_4, (b) Interconnecting forces ($\boldsymbol{\mu}$) and interface displacement ($\mathbf{u}_b^{(k)}$), (c) Assembled FE model Ω with its interface boundary Γ.

in which $\mathbf{U}_b^{(k)}$ is the interface displacement vector of the k^{th} substructure, and $\mathbf{b}^{(k)}$ is a signed Boolean matrix.

Using the linear dynamic equations for each substructure in Eq. (13) and the compatibility constraint equation in Eq. (14), the dynamic equilibrium equation of the global FE model (see Fig. 2c) is assembled as

$$\begin{bmatrix} \mathbf{M} & \mathbf{0} \\ \mathbf{0} & \mathbf{0} \end{bmatrix} \begin{bmatrix} \ddot{\mathbf{U}} \\ \ddot{\boldsymbol{\gamma}} \end{bmatrix} + \begin{bmatrix} \mathbf{K} & \mathbf{B} \\ \mathbf{B}^T & \mathbf{0} \end{bmatrix} \begin{bmatrix} \mathbf{U} \\ \boldsymbol{\gamma} \end{bmatrix} = \begin{bmatrix} \mathbf{f} \\ \mathbf{0} \end{bmatrix}, \tag{15a}$$

$$\text{with } \mathbf{M} = \begin{bmatrix} \mathbf{M}^{(1)} & & \mathbf{0} \\ & \ddots & \\ \mathbf{0} & & \mathbf{M}^{(N_s)} \end{bmatrix}, \mathbf{K} = \begin{bmatrix} \mathbf{K}^{(1)} & & \mathbf{0} \\ & \ddots & \\ \mathbf{0} & & \mathbf{K}^{(N_s)} \end{bmatrix}, \mathbf{U} = \begin{bmatrix} \mathbf{U}^{(1)} \\ \vdots \\ \mathbf{U}^{(N_s)} \end{bmatrix}, \mathbf{f} = \begin{bmatrix} \mathbf{f}^{(1)} \\ \vdots \\ \mathbf{f}^{(N_s)} \end{bmatrix}, \mathbf{B} = \begin{bmatrix} \mathbf{B}^{(1)} \\ \vdots \\ \mathbf{B}^{(N_s)} \end{bmatrix}, \tag{15b}$$

where $\mathbf{M}$ and $\mathbf{K}$ are the block-diagonal mass and stiffness matrices that consist of the substructural mass and stiffness matrices ($\mathbf{M}^{(k)}$ and $\mathbf{K}^{(k)}$).

Then, the global eigenpairs are obtained from the following eigenvalue problem

$$\mathbf{K}_g(\boldsymbol{\varphi}_g)_i = (\lambda_g)_i \mathbf{M}_g(\boldsymbol{\varphi}_g)_i \quad \text{for } i = 1, \cdots, N_g, \tag{16a}$$

$$\text{with } \mathbf{M}_g = \begin{bmatrix} \mathbf{M} & \mathbf{0} \\ \mathbf{0} & \mathbf{0} \end{bmatrix}, \mathbf{K}_g = \begin{bmatrix} \mathbf{K} & \mathbf{B} \\ \mathbf{B}^T & \mathbf{0} \end{bmatrix}, \tag{16b}$$

in which $(\lambda_g)_i$ and $(\boldsymbol{\varphi}_g)_i$ are the global eigenvalue and eigenvector of the i^{th} global mode, respectively, and N_g is the number of DOFs in the assembled global FE model. This number is the sum of the numbers of interface and substructural DOFs ($N_g = N_\mu + \sum_{k=1}^{N_s} N^{(k)}$, where N_μ is the number of Lagrange multipliers and $N^{(k)}$ is the number of DOFs in the k^{th} substructure).

3.2. Substructural reduction

In Eq. (15), the dynamic equilibrium equations corresponding to the k^{th} substructure can be extracted as

$$\begin{bmatrix} \mathbf{M}^{(k)} & \mathbf{0} \\ \mathbf{0} & \mathbf{0} \end{bmatrix} \begin{bmatrix} \ddot{\mathbf{U}}^{(k)} \\ \ddot{\boldsymbol{\gamma}} \end{bmatrix} + \begin{bmatrix} \mathbf{K}^{(k)} & \mathbf{B}^{(k)} \\ \mathbf{B}^{(k)T} & \mathbf{0} \end{bmatrix} \begin{bmatrix} \mathbf{U}^{(k)} \\ \boldsymbol{\gamma} \end{bmatrix} = \begin{bmatrix} \mathbf{f}^{(k)} \\ \mathbf{0} \end{bmatrix}, \tag{17}$$

and then the eigenvalue problem of the k^{th} substructure is given by

$$\begin{bmatrix} \mathbf{K}^{(k)} & \mathbf{B}^{(k)} \\ \mathbf{B}^{(k)T} & \mathbf{0} \end{bmatrix} \begin{bmatrix} \mathbf{u}^{(k)} \\ \boldsymbol{\mu} \end{bmatrix} = \lambda^{(k)} \begin{bmatrix} \mathbf{M}^{(k)} & \mathbf{0} \\ \mathbf{0} & \mathbf{0} \end{bmatrix} \begin{bmatrix} \mathbf{u}^{(k)} \\ \boldsymbol{\mu} \end{bmatrix}, \tag{18}$$

in which $\mathbf{u}^{(k)}$ and $\boldsymbol{\mu}$ are the eigenvectors corresponding to the substructural displacement vector $\mathbf{U}^{(k)}$ and the Lagrange multiplier vector $\boldsymbol{\gamma}$, respectively, and $\lambda^{(k)}$ is the eigenvalue of the k^{th} substructure.

The substructural quantities ($\mathbf{M}^{(k)}$, $\mathbf{K}^{(k)}$, $\mathbf{B}^{(k)}$, and $\mathbf{u}^{(k)}$) are decomposed into master and slave parts as follows

$$\mathbf{M}^{(k)} = \begin{bmatrix} \mathbf{M}_{ss}^{(k)} & \mathbf{M}_{sm}^{(k)} \\ \mathbf{M}_{ms}^{(k)} & \mathbf{M}_{mm}^{(k)} \end{bmatrix}, \mathbf{K}^{(k)} = \begin{bmatrix} \mathbf{K}_{ss}^{(k)} & \mathbf{K}_{sm}^{(k)} \\ \mathbf{K}_{ms}^{(k)} & \mathbf{K}_{mm}^{(k)} \end{bmatrix}, \mathbf{B}^{(k)} = \begin{bmatrix} \mathbf{B}_s^{(k)} \\ \mathbf{B}_m^{(k)} \end{bmatrix}, \mathbf{u}^{(k)} = \begin{bmatrix} \mathbf{u}_s^{(k)} \\ \mathbf{u}_m^{(k)} \end{bmatrix}, \tag{19}$$

where the master DOFs are selected by using the ratio of the diagonal components of mass and stiffness matrices [34,35].

Substituting Eq. (19) into Eq. (18), the eigenvalue problem of the k^{th} substructure can be rewritten as

$$\begin{bmatrix} \mathbf{K}_{ss}^{(k)} & \mathbf{K}_{sm}^{(k)} & \mathbf{B}_s^{(k)} \\ \mathbf{K}_{ms}^{(k)} & \mathbf{K}_{mm}^{(k)} & \mathbf{B}_m^{(k)} \\ \mathbf{B}_s^{(k)T} & \mathbf{B}_m^{(k)T} & \mathbf{0} \end{bmatrix} \begin{bmatrix} \mathbf{u}_s^{(k)} \\ \mathbf{u}_m^{(k)} \\ \boldsymbol{\mu} \end{bmatrix} = \lambda^{(k)} \begin{bmatrix} \mathbf{M}_{ss}^{(k)} & \mathbf{M}_{sm}^{(k)} & \mathbf{0} \\ \mathbf{M}_{ms}^{(k)} & \mathbf{M}_{mm}^{(k)} & \mathbf{0} \\ \mathbf{0} & \mathbf{0} & \mathbf{0} \end{bmatrix} \begin{bmatrix} \mathbf{u}_s^{(k)} \\ \mathbf{u}_m^{(k)} \\ \boldsymbol{\mu} \end{bmatrix}. \tag{20}$$

From the first row in Eq. (20), $\mathbf{u}_s^{(k)}$ is represented by

$$\mathbf{u}_s^{(k)} = -(\mathbf{K}_{ss}^{(k)} - \lambda^{(k)} \mathbf{M}_{ss}^{(k)})^{-1} [(\mathbf{K}_{sm}^{(k)} - \lambda^{(k)} \mathbf{M}_{sm}^{(k)}) \mathbf{u}_m^{(k)} + \mathbf{B}_s^{(k)} \boldsymbol{\mu}]. \tag{21}$$

Eq. (21) can be expanded by a Neumann series [13–20]. Neglecting terms higher than the order of $\lambda^{(k)}$, the slave displacement vector is approximated as

$$\mathbf{u}_s^{(k)} \approx \bar{\mathbf{u}}_s^{(k)} = [\mathbf{P}_s^{(k)} + \lambda^{(k)} \boldsymbol{\Theta}_s^{(k)}] \mathbf{u}_m^{(k)} + (\mathbf{P}_\mu^{(k)} + \lambda^{(k)} \boldsymbol{\Theta}_\mu^{(k)}) \boldsymbol{\mu}, \tag{22}$$

with

$$\mathbf{P}_s^{(k)} = -(\mathbf{K}_{ss}^{(k)})^{-1}\mathbf{K}_{sm}^{(k)},\ \boldsymbol{\Theta}_s^{(k)} = (\mathbf{K}_{ss}^{(k)})^{-1}(\mathbf{M}_{sm}^{(k)} + \mathbf{M}_{ss}^{(k)}\mathbf{P}_s^{(k)}), \tag{23a}$$

$$\mathbf{P}_\mu^{(k)} = -(\mathbf{K}_{ss}^{(k)})^{-1}\mathbf{B}_s^{(k)},\ \boldsymbol{\Theta}_\mu^{(k)} = (\mathbf{K}_{ss}^{(k)})^{-1}\mathbf{M}_{ss}^{(k)}\mathbf{P}_\mu^{(k)}. \tag{23b}$$

Then, using $\bar{\mathbf{u}}_s^{(k)}$ instead of $\mathbf{u}_s^{(k)}$, the eigenvector of the k^{th} substructure in Eq. (20) is approximated as

$$\begin{bmatrix}\mathbf{u}_s^{(k)}\\ \mathbf{u}_m^{(k)}\\ \boldsymbol{\mu}\end{bmatrix} \approx \begin{bmatrix}\bar{\mathbf{u}}_s^{(k)}\\ \mathbf{u}_m^{(k)}\\ \boldsymbol{\mu}\end{bmatrix} = \mathbf{T}_0^{(k)}\begin{bmatrix}\mathbf{u}_m^{(k)}\\ \boldsymbol{\mu}\end{bmatrix} + \lambda^{(k)}\mathbf{T}_a^{(k)}\begin{bmatrix}\mathbf{u}_m^{(k)}\\ \boldsymbol{\mu}\end{bmatrix}, \tag{24a}$$

$$\text{with}\ \ \mathbf{T}_0^{(k)} = \begin{bmatrix}\mathbf{P}_s^{(k)} & \mathbf{P}_\mu^{(k)}\\ \mathbf{I}_m^{(k)} & \mathbf{0}\\ \mathbf{0} & \mathbf{I}_\mu\end{bmatrix},\ \mathbf{T}_a^{(k)} = \begin{bmatrix}\boldsymbol{\Theta}_s^{(k)} & \boldsymbol{\Theta}_\mu^{(k)}\\ \mathbf{0} & \mathbf{0}\\ \mathbf{0} & \mathbf{0}\end{bmatrix}, \tag{24b}$$

where $\mathbf{T}_0^{(k)}$ is the Guyan transformation matrix reflecting the free interface substructuring, $\mathbf{T}_a^{(k)}$ is the additional transformation matrix containing the inertial effects of the slave DOFs of the k^{th} substructure. Here, $\mathbf{I}_m^{(k)}$ and $\mathbf{I}_\mu$ are the identity matrices corresponding to the master DOFs of the k^{th} substructure and Lagrange multiplier, respectively.

Considering only the transformation matrix $\mathbf{T}_0^{(k)}$ in Eq. (24b), the eigenvalue problem corresponding to the k^{th} substructure in Eq. (20) is reduced as follows

$$\bar{\mathbf{K}}_0^{(k)}\begin{bmatrix}\mathbf{u}_m^{(k)}\\ \boldsymbol{\mu}\end{bmatrix} = \bar{\lambda}^{(k)}\bar{\mathbf{M}}_0^{(k)}\begin{bmatrix}\mathbf{u}_m^{(k)}\\ \boldsymbol{\mu}\end{bmatrix}, \tag{25a}$$

$$\text{with}\ \ \bar{\mathbf{M}}_0^{(k)} = \mathbf{T}_0^{(k)T}\begin{bmatrix}\mathbf{M}^{(k)} & \mathbf{0}\\ \mathbf{0} & \mathbf{0}\end{bmatrix}\mathbf{T}_0^{(k)},\ \bar{\mathbf{K}}_0^{(k)} = \mathbf{T}_0^{(k)T}\begin{bmatrix}\mathbf{K}^{(k)} & \mathbf{B}^{(k)}\\ \mathbf{B}^{(k)T} & \mathbf{0}\end{bmatrix}\mathbf{T}_0^{(k)}, \tag{25b}$$

in which $\bar{\lambda}^{(k)}$ is the approximated eigenvalue of the k^{th} substructure.

Pre-multiplying $(\bar{\mathbf{M}}_0^{(k)})^{-1}$ on the both sides of Eq. (25a), the following relation is obtained

$$\bar{\lambda}^{(k)}\begin{bmatrix}\mathbf{u}_m^{(k)}\\ \boldsymbol{\mu}\end{bmatrix} = \mathbf{H}^{(k)}\begin{bmatrix}\mathbf{u}_m^{(k)}\\ \boldsymbol{\mu}\end{bmatrix}\ \text{with}\ \mathbf{H}^{(k)} = (\bar{\mathbf{M}}_0^{(k)})^{-1}\bar{\mathbf{K}}_0^{(k)}. \tag{26}$$

Substituting Eq. (26) into Eq. (24a), the approximated eigenvector of the k^{th} substructure is redefined as

$$\begin{bmatrix}\bar{\mathbf{u}}_s^{(k)}\\ \mathbf{u}_m^{(k)}\\ \boldsymbol{\mu}\end{bmatrix} = \mathbf{T}_1^{(k)}\begin{bmatrix}\mathbf{u}_m^{(k)}\\ \boldsymbol{\mu}\end{bmatrix}\ \text{with}\ \mathbf{T}_1^{(k)} = \mathbf{T}_0^{(k)} + \mathbf{T}_a^{(k)}\mathbf{H}^{(k)}, \tag{27}$$

where $\mathbf{T}_1^{(k)}$ is the transformation matrix of the proposed method. Here, $\mathbf{H}^{(k)}$ is decomposed into the master and Lagrange multiplier parts as follows:

$$\mathbf{H}^{(k)} = \begin{bmatrix}\mathbf{H}_{mm}^{(k)} & \mathbf{H}_{m\mu}^{(k)}\\ \mathbf{H}_{\mu m}^{(k)} & \mathbf{H}_{\mu\mu}^{(k)}\end{bmatrix}. \tag{28}$$

From Eqs. (24b), (27), and (28), $\mathbf{T}_1^{(k)}$ can be expressed as

$$\mathbf{T}_1^{(k)} = \begin{bmatrix}\mathbf{A}^{(k)} & \boldsymbol{\Psi}^{(k)}\\ \mathbf{0} & \mathbf{I}_\mu\end{bmatrix}\ \text{with}\ \mathbf{A}^{(k)} = \begin{bmatrix}\hat{\mathbf{P}}_s^{(k)}\\ \mathbf{I}_m^{(k)}\end{bmatrix},\ \boldsymbol{\Psi}^{(k)} = \begin{bmatrix}\hat{\mathbf{P}}_\mu^{(k)}\\ \mathbf{0}\end{bmatrix}, \tag{29}$$

in which the component matrices $\hat{\mathbf{P}}_s^{(k)}$ and $\hat{\mathbf{P}}_\mu^{(k)}$ are calculated as

$$\hat{\mathbf{P}}_s^{(k)} = \mathbf{P}_s^{(k)} + \boldsymbol{\Theta}_s^{(k)}\mathbf{H}_{mm}^{(k)} + \boldsymbol{\Theta}_\mu^{(k)}\mathbf{H}_{\mu m}^{(k)},\ \hat{\mathbf{P}}_\mu^{(k)} = \mathbf{P}_\mu^{(k)} + \boldsymbol{\Theta}_s^{(k)}\mathbf{H}_{m\mu}^{(k)} + \boldsymbol{\Theta}_\mu^{(k)}\mathbf{H}_{\mu\mu}^{(k)}. \tag{30}$$

The reduced substructural system matrices are calculated as

$$\bar{\mathbf{M}}_1^{(k)} = \mathbf{T}_1^{(k)T}\begin{bmatrix}\mathbf{M}^{(k)} & \mathbf{0}\\ \mathbf{0} & \mathbf{0}\end{bmatrix}\mathbf{T}_1^{(k)},\ \bar{\mathbf{K}}_1^{(k)} = \mathbf{T}_1^{(k)T}\begin{bmatrix}\mathbf{K}^{(k)} & \mathbf{B}^{(k)}\\ \mathbf{B}^{(k)T} & \mathbf{0}\end{bmatrix}\mathbf{T}_1^{(k)}, \tag{31}$$

and considering the master DOFs and Lagrange multipliers, $\bar{\mathbf{M}}_1^{(k)}$ and $\bar{\mathbf{K}}_1^{(k)}$ are decomposed as

$$\bar{\mathbf{M}}_1^{(k)} = \begin{bmatrix} \bar{\mathbf{M}}_{mm}^{(k)} & \bar{\mathbf{M}}_{m\mu}^{(k)} \\ \bar{\mathbf{M}}_{\mu m}^{(k)} & \bar{\mathbf{M}}_{\mu\mu}^{(k)} \end{bmatrix}, \bar{\mathbf{K}}_1^{(k)} = \begin{bmatrix} \bar{\mathbf{K}}_{mm}^{(k)} & \bar{\mathbf{K}}_{m\mu}^{(k)} \\ \bar{\mathbf{K}}_{\mu m}^{(k)} & \bar{\mathbf{K}}_{\mu\mu}^{(k)} \end{bmatrix}. \tag{32}$$

Then, after obtaining Eq. (32) for all substructures, the reduced mass and stiffness matrices for the global FE model considered is simply assembled as follows

Table 1
Algorithm of the proposed method.

Algorithm. A dynamic condensation method with free interface substructuring

for $k = 1, 2, \ldots N_s$,
  load the substructural system matrices ($\mathbf{M}^{(k)}$, $\mathbf{K}^{(k)}$, $\mathbf{B}^{(k)}$) in Eq. (18)
  do the DOF decomposition by Eq. (19)
  compute the transformation matrices $\mathbf{T}_0^{(k)}$ by Eqs. (23) and (24)
  do the substructural static pre-condensation ($\bar{\mathbf{M}}_0^{(k)}$, $\bar{\mathbf{K}}_0^{(k)}$) by Eq. (25)
  compute $\mathbf{H}^{(k)}$ to approximate the unknown $\lambda^{(k)}$ by Eq. (26)
  compute $\mathbf{T}_a^{(k)}$ and $\mathbf{T}_1^{(k)}$ by Eqs. (23), (24) and (29)
  do the substructural dynamic condensation ($\bar{\mathbf{M}}_1^{(k)}$, $\bar{\mathbf{K}}_1^{(k)}$) by Eq. (31)
  do the DOF decomposition for the reduced system matrices by Eq. (32)
end for
assemble all the substructural reduced matrices by Eq. (33)
solve the reduced eigenvalue problem in Eq. (34)
compute the approximated eigenvector by Eq. (35)

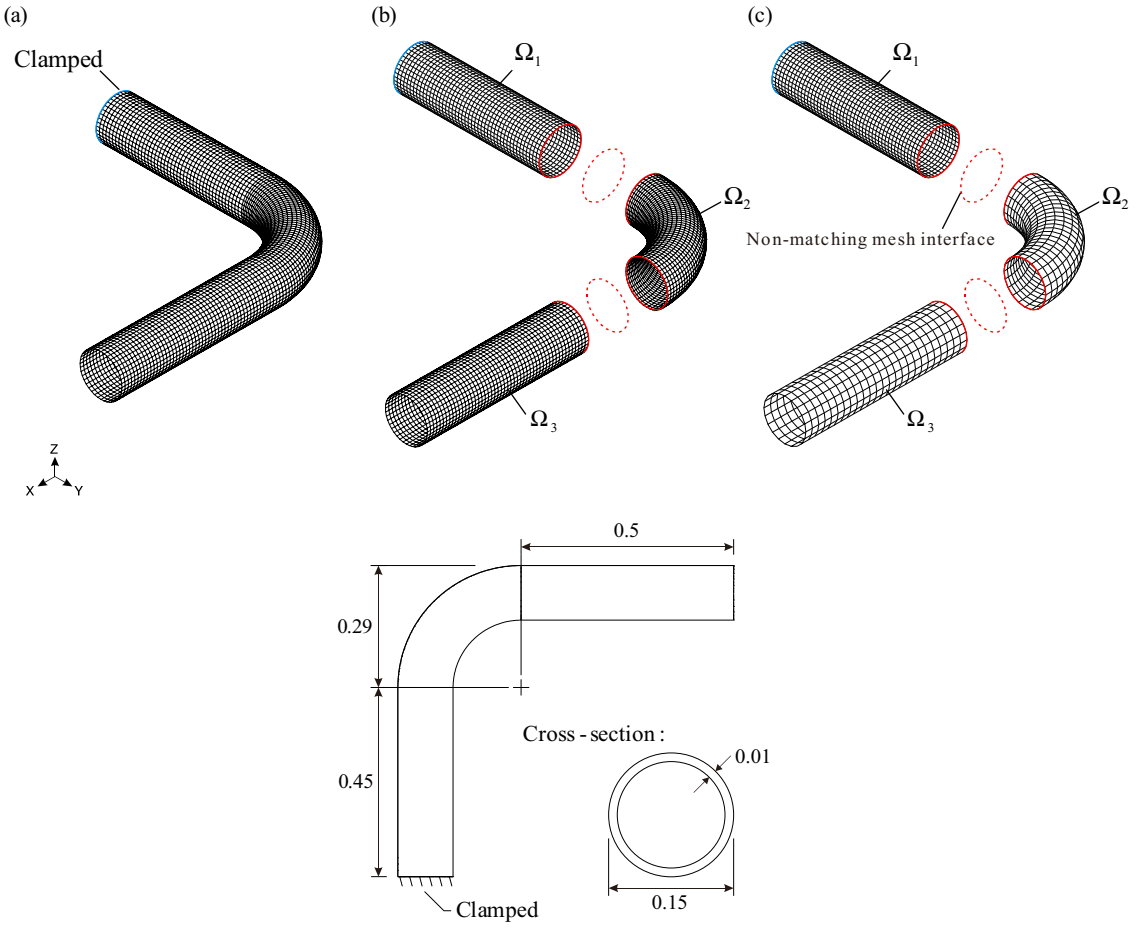

Fig. 3. Bended pipe problem: (a) FE model without substructuring, (b) Matching mesh on the interface, (c) Non-matching mesh between neighboring substructures.

$$\overline{\mathbf{M}} = \begin{bmatrix} \overline{\mathbf{M}}_{mm}^{(1)} & & \mathbf{0} & \overline{\mathbf{M}}_{m\mu}^{(1)} \\ & \ddots & & \vdots \\ \mathbf{0} & & \overline{\mathbf{M}}_{mm}^{(N_s)} & \overline{\mathbf{M}}_{m\mu}^{(N_s)} \\ \overline{\mathbf{M}}_{\mu m}^{(1)} & \cdots & \overline{\mathbf{M}}_{\mu m}^{(N_s)} & \overline{\mathbf{M}}_{\mu\mu} \end{bmatrix}, \quad \overline{\mathbf{K}} = \begin{bmatrix} \overline{\mathbf{K}}_{mm}^{(1)} & & \mathbf{0} & \overline{\mathbf{K}}_{m\mu}^{(1)} \\ & \ddots & & \vdots \\ \mathbf{0} & & \overline{\mathbf{K}}_{mm}^{(N_s)} & \overline{\mathbf{K}}_{m\mu}^{(N_s)} \\ \overline{\mathbf{K}}_{\mu m}^{(1)} & \cdots & \overline{\mathbf{K}}_{\mu m}^{(N_s)} & \overline{\mathbf{K}}_{\mu\mu} \end{bmatrix}, \tag{33a}$$

$$\text{with} \quad \bar{\mathbf{M}}_{\mu\mu} = \sum_{k=1}^{N_s} \bar{\mathbf{M}}_{\mu\mu}^{(k)}, \; \bar{\mathbf{K}}_{\mu\mu} = \sum_{k=1}^{N_s} \bar{\mathbf{K}}_{\mu\mu}^{(k)}, \tag{33b}$$

in which $\bar{\mathbf{M}}$ and $\bar{\mathbf{K}}$ are $N_1 \times N_1$ matrices, and N_1 is the number of DOFs in the reduced FE model: $N_1 = N_\mu + \sum_{k=1}^{N_s} N_m^{(k)}$ and $N_m^{(k)}$ is the number of master DOFs of the k^{th} substructure.

Using the proposed method, the reduced eigenvalue problem is given by

$$\bar{\mathbf{K}}(\bar{\boldsymbol{\varphi}})_i = \bar{\lambda}_i \bar{\mathbf{M}}(\bar{\boldsymbol{\varphi}})_i, \; i = 1, 2, \cdots, N_1, \tag{34}$$

where $\bar{\lambda}_i$ and $(\bar{\boldsymbol{\varphi}})_i$ are the approximated i^{th} eigenvalues and the corresponding eigenvectors.

The approximated global eigenvector $(\bar{\boldsymbol{\varphi}}_g)_i$ can be calculated by

$$(\overline{\boldsymbol{\varphi}}_g)_i = \overline{\mathbf{T}}(\overline{\boldsymbol{\varphi}})_i \quad \text{with} \quad \overline{\mathbf{T}} = \begin{bmatrix} \mathbf{A}^{(1)} & & \mathbf{0} & \boldsymbol{\Psi}^{(1)} \\ & \ddots & & \vdots \\ \mathbf{0} & & \mathbf{A}^{(N_s)} & \boldsymbol{\Psi}^{(N_s)} \\ \mathbf{0} & \cdots & \mathbf{0} & \mathbf{I}_\mu \end{bmatrix}, \tag{35}$$

in which $\bar{\mathbf{T}}$ is assembled using the transformation matrices $\mathbf{T}_1^{(k)}$ already calculated in Eq. (29).

We summarize the algorithm of the proposed method in Table 1. In the following sections, the performance of the proposed method is investigated using various numerical examples.

Table 2
Number of master DOFs used and number of DOFs used in original and reduced models for the bended pipe problem.

Cases	Methods	$N_m^{(1)}$	$N_m^{(2)}$	$N_m^{(3)}$	N_m	N_b	N_g	N_1
Matching mesh	Guyan	–	–	–	2340	–	28200	2340
	IRS	–	–	–	2340	–	28200	2340
	Proposed	560	775	605	1940	400	29000	2340
Non-matching mesh	Proposed	470	270	175	915	300	14300	1215

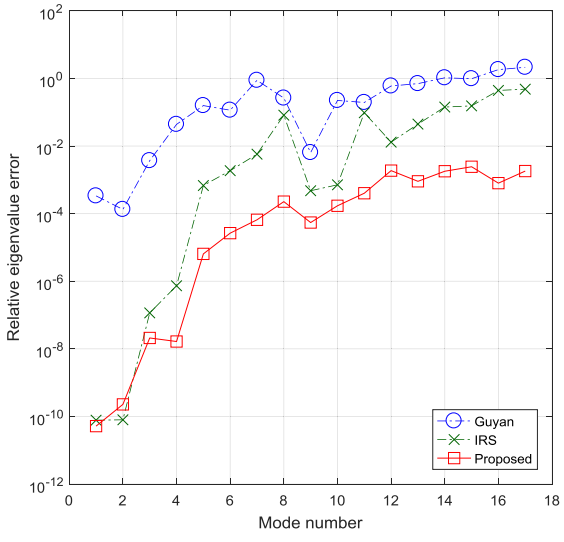

Fig. 4. Relative eigenvalue errors in the bended pipe problem with matching mesh, as shown in Fig. 3a and b.

4. Numerical examples

In this section, we investigate the performance of the proposed method. Three structural problems are considered: a bended pipe, a NACA 2415 airfoil structure, and a wind-turbine rotor.

All finite element models are constructed using the 4-node MITC (Mixed Interpolation of Tensorial Components) shell elements [36–41], and free or fixed boundary conditions are imposed differently according to the problem. All the computer codes are implemented in MATLAB and computation was performed in a personal computer (Inter core (TM) i7-4770, 3.40 GHz CPU, 32 GB RAM).

The relative eigenvalue error is adopted to measure the accuracy of the reduced models

$$\xi_i = \frac{\left|\lambda_i - \bar{\lambda}_i\right|}{\lambda_i}, \tag{36}$$

Table 3
Computational costs for the bended pipe problem in Fig. 4.

Methods	Items	Computation times	
		[s]	Ratio [%]
IRS	Load system matrices ($\mathbf{M}_g$,$\mathbf{K}_g$)	0.09	0.01
	DOF decomposition (master & slave DOFs)	0.12	0.02
	Static pre-condensation	576.98	80.69
	Dynamic condensation	137.90	19.28
	Total	715.09	100.00
Proposed	Load system matrices ($\mathbf{M}^{(i)}$, $\mathbf{K}^{(i)}$,$\mathbf{B}^{(i)}$) (Line 2 in Algorithm, see Table 1)	0.22	0.03
	DOF decomposition (master & slave DOFs) (Line 3)	0.07	0.01
	Substructural static pre-condensation (Line 4–5)	105.48	14.75
	Substructural dynamic condensation (Line 6–9)	159.76	22.34
	Assemble the all substructural reduced matrices (Line 11)	0.12	0.02
	Total	265.65	37.15

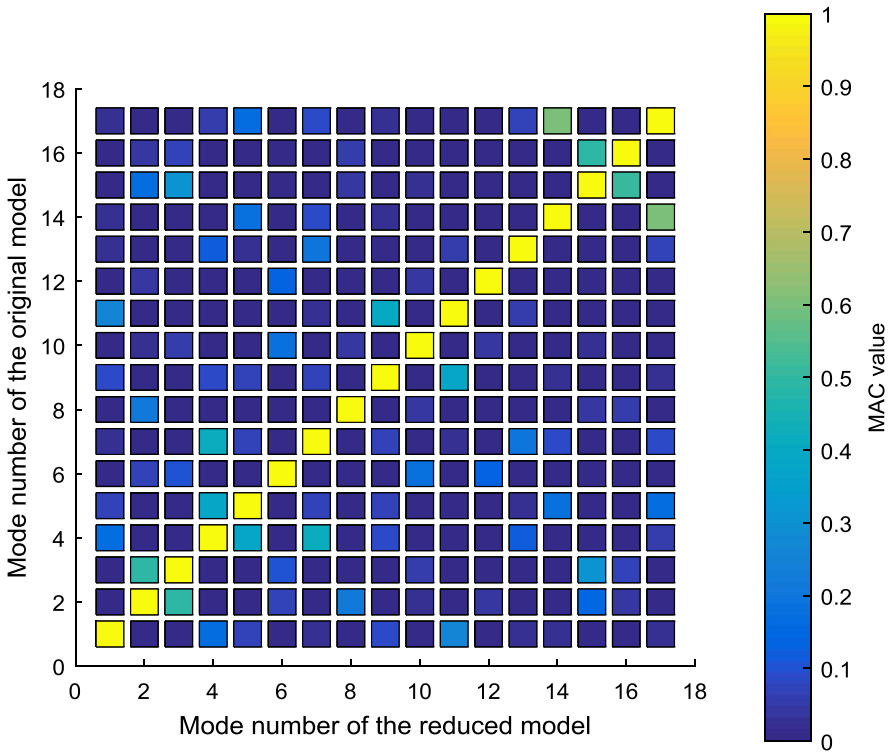

Fig. 5. MAC for the reduced model obtained using the proposed method in the bended pipe problem with matching mesh shown in Fig. 3b.

in which ξ_i is the i^{th} relative eigenvalue error, λ_i is the i^{th} exact eigenvalue calculated from the global eigenvalue problem in Eq. (16); and $\bar{\lambda}_i$ is the i^{th} approximated eigenvalue calculated from the reduced eigenvalue problem.

The accuracy of approximated eigenvectors is measured by the modal assurance criterion (MAC) [42–43]

$$\mathrm{MAC}(i,j) = \frac{|(\boldsymbol{\varphi}_g)_i^T(\bar{\boldsymbol{\varphi}}_g)_j|^2}{((\boldsymbol{\varphi}_g)_i^T(\boldsymbol{\varphi}_g)_i)((\bar{\boldsymbol{\varphi}}_g)_j^T(\bar{\boldsymbol{\varphi}}_g)_j)} \quad \text{for } i,j = 1,2,\cdots,N_1, \tag{37}$$

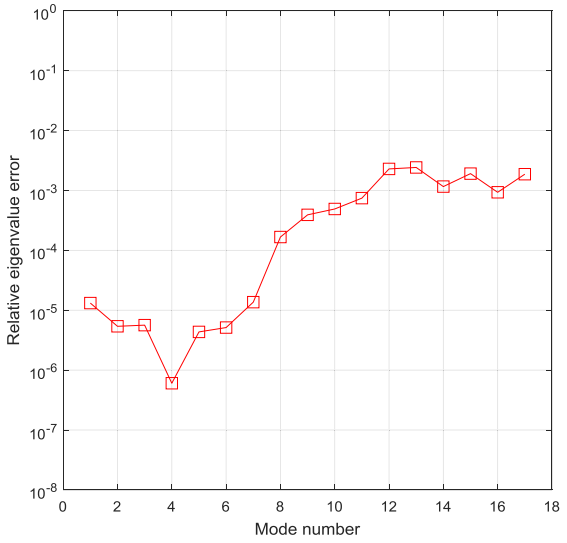

Fig. 6. Relative eigenvalue errors in the bended pipe problem with non-matching mesh shown in Fig. 3c.

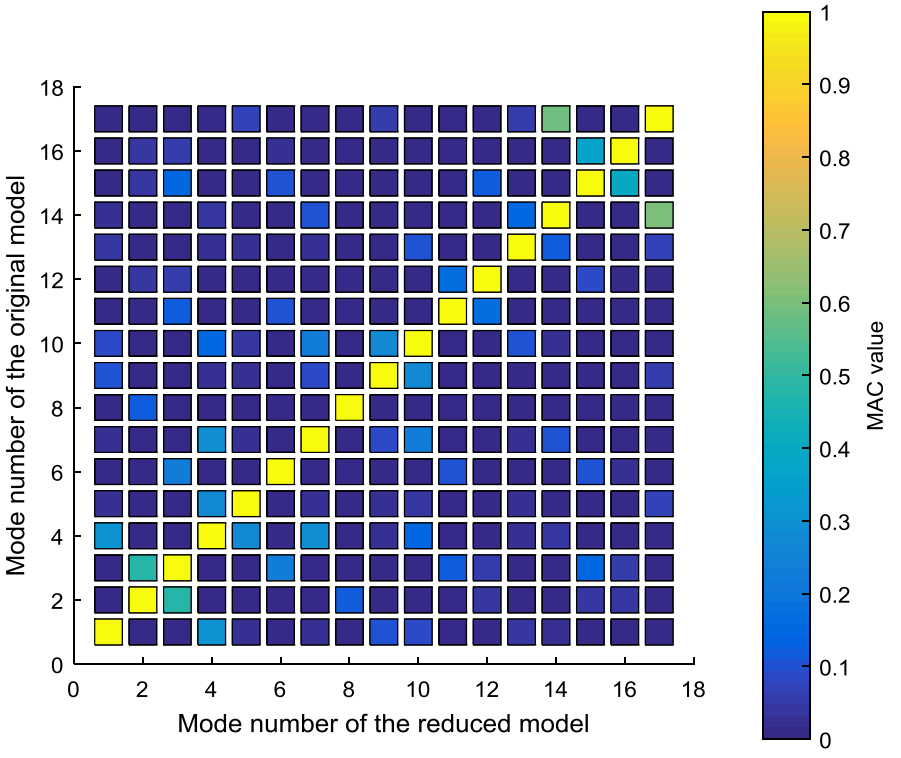

Fig. 7. MAC for the reduced model obtained using the proposed method in the bended pipe problem with non-matching mesh in Fig. 3c.

in which $(\boldsymbol{\varphi}_g)$ and $(\bar{\boldsymbol{\varphi}}_g)$ are the original and approximated eigenvectors calculated by Eqs. (16) and (34), respectively. The resulting MAC values are assembled to form the MAC matrix. The MAC values indicate the consistency between eigenvectors using values from zero to unity. If the MAC value is near unity, the eigenvectors are considered consistent.

4.1. Bended pipe problem

A bended pipe structure with clamped boundary at one end is considered as shown in Fig. 3, in which the structural configuration and its FE models are illustrated. Young's modulus E is 69 GPa, Poisson's ratio ν is 0.35, and density ρ is

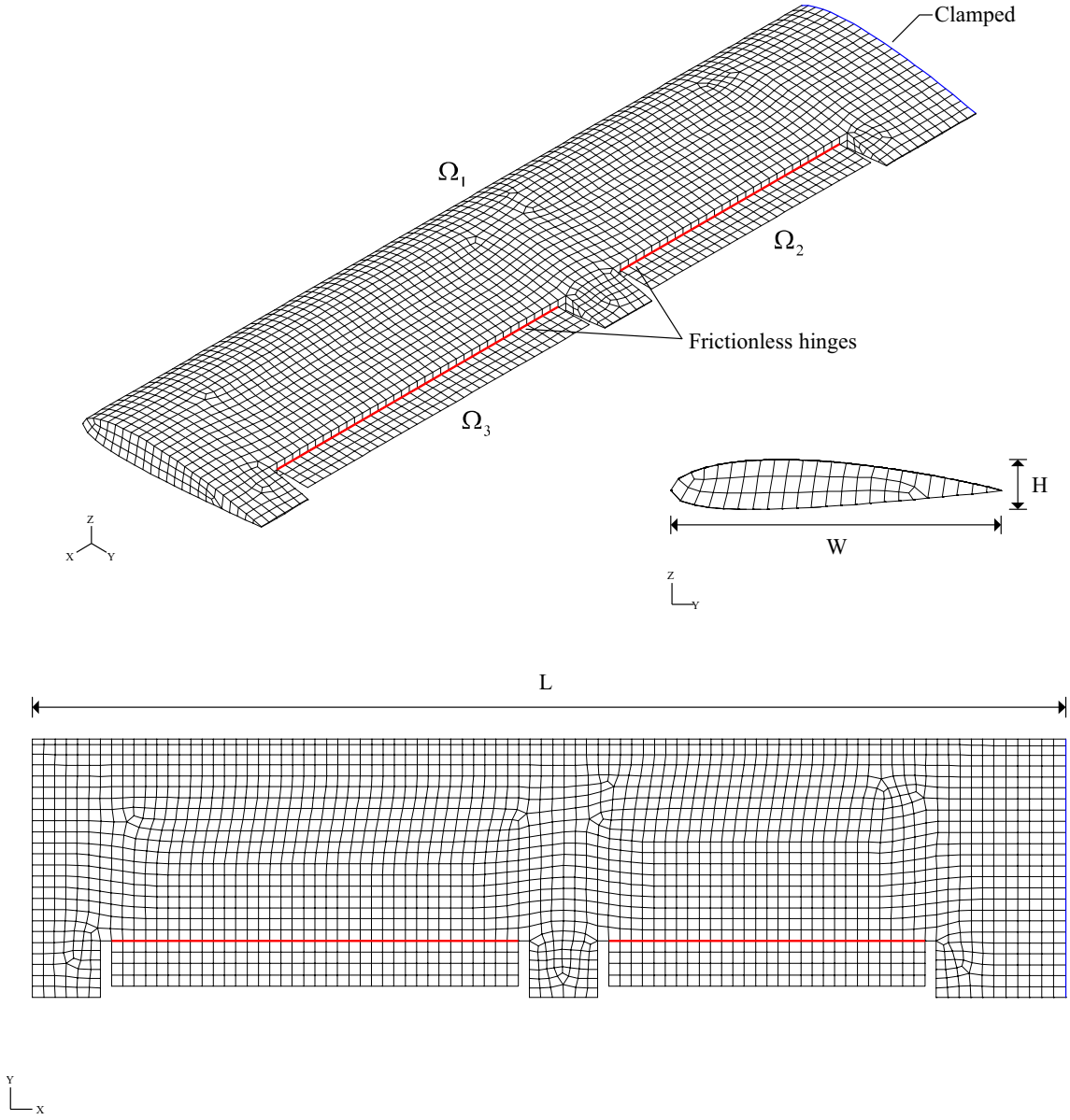

Fig. 8. NACA 2415 airfoil structure problem.

Table 4
Number of master DOFs used and number of DOFs used in the original and reduced models for the NACA 2415 airfoil structure problem.

$N_m^{(1)}$	$N_m^{(2)}$	$N_m^{(3)}$	N_m	N_b	N_g	N_1
1675	195	245	2115	198	21098	2313

2700 kg/m^3. The structure is an assemblage of three substructures ($N_s = 3$). We consider the FE models with matching and non-matching meshes between neighboring substructures. The detailed numbers of DOFs used in original and reduced models are listed in Table 2. Note that the rigid body modes are not considered in measuring the accuracy.

For the matching mesh model, the structure is modeled using 5640 shell elements. In this problem, we investigate the accuracy and computational efficiency of the proposed method compared to the Guyan reduction and IRS methods. The Guyan reduction and IRS methods are used for the FE model without substructuring in Fig. 3a and the reduced model of size $N_1 = 2340$ ($N_m = 2340$) is obtained. The proposed method is employed for the FE model with substructuring in Fig. 3b,

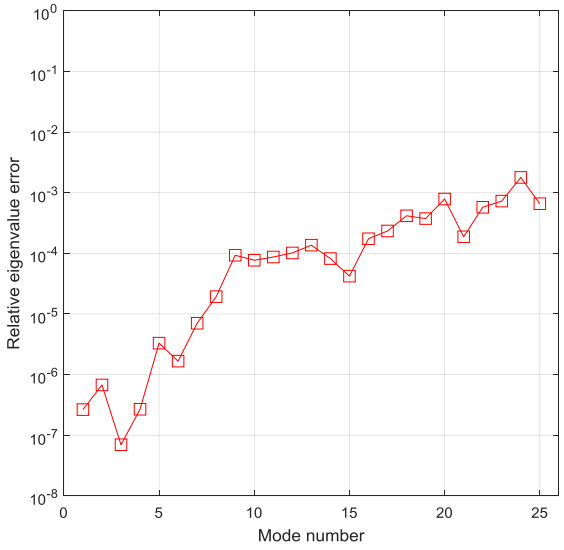

Fig. 9. Relative eigenvalue errors in the NACA 2415 airfoil structure problem.

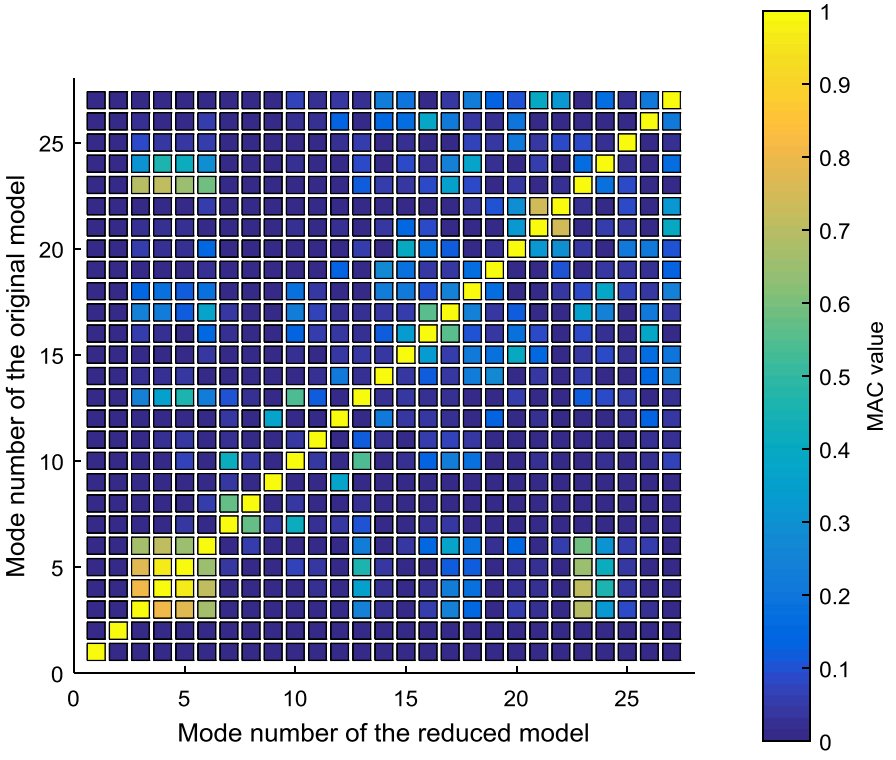

Fig. 10. MAC for the reduced model obtained using the proposed method in the NACA 2415 airfoil structure problem.

resulting in the reduced model of size $N_1 = 2340$ ($N_m = 1940$). The reduced models have the same size for all three methods adopted.

Fig. 4 presents the relative eigenvalue errors corresponding to the 1st–17th modes obtained by the Guyan, IRS, and proposed methods. Table 3 presents the detailed computational cost. For reduced models of the same size, the computational

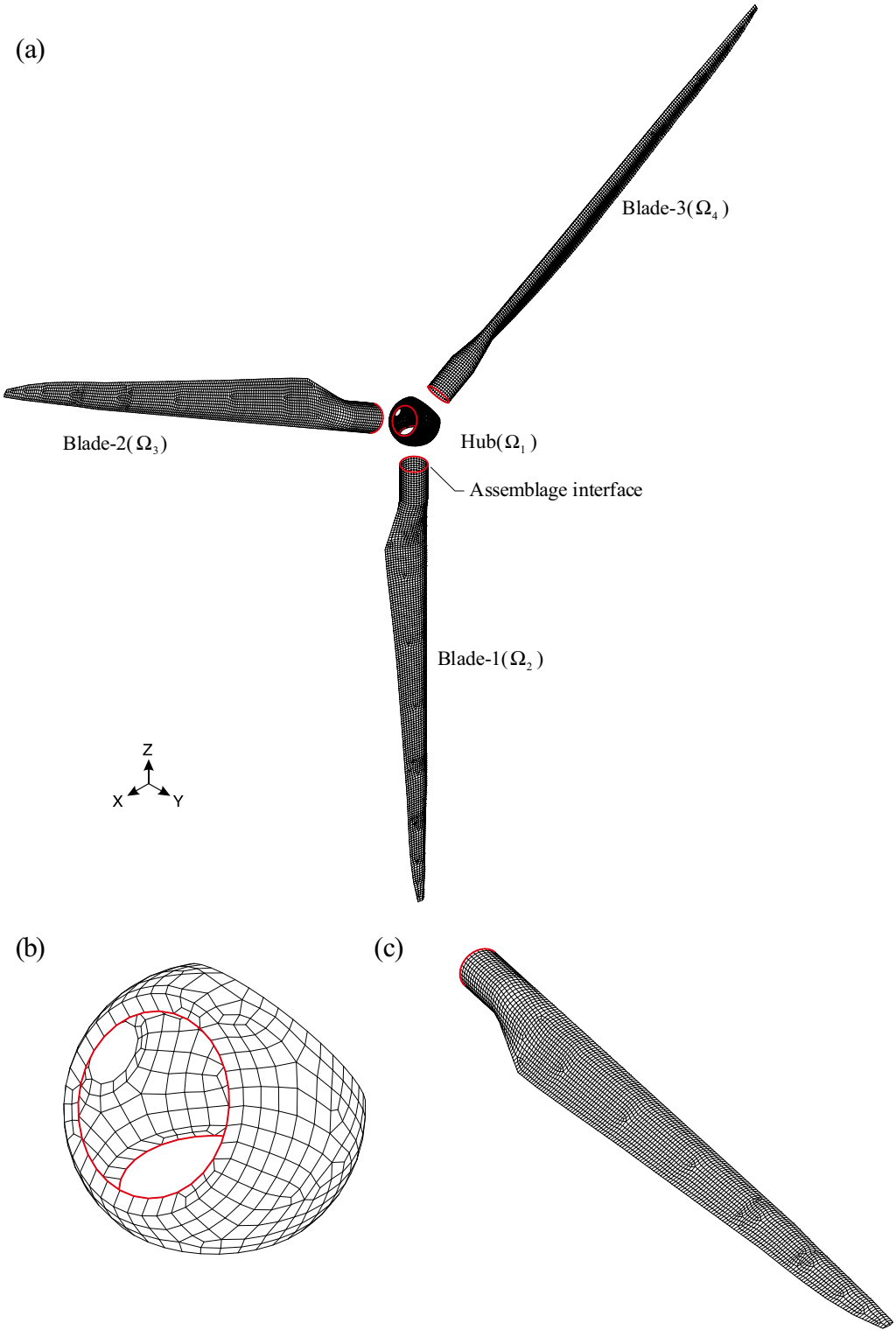

Fig. 11. Wind-turbine rotor problem.

cost of the proposed method is only 37.15% that of the IRS method and produces greater accuracy than the Guyan and IRS methods do. Fig. 5 presents the MAC for the reduced model obtained using the proposed method. The approximated eigenvectors calculated by the proposed method are highly consistent with the eigenvectors of the original model.

Let us consider the non-matching mesh case shown in Fig. 3c. The substructures are modeled using 1800 (Ω_1), 460 (Ω_2), and 500 (Ω_3) shell elements, respectively. Non-matching mesh is located at the interface between substructures, Ω_1 and Ω_2. The proposed method is used with a reduced model of size $N_1 = 1215$ ($N_m = 915$). Note that the Guyan reduction and IRS methods cannot be used for cases in which the meshes are non-matching.

Fig. 6 presents the relative eigenvalue errors obtained by the proposed method. The results show the accuracy of the proposed method for this case of non-matching meshes. Fig. 7 presents the MAC for the reduced model. The approximated eigenvectors also maintain good consistency when compared to the eigenvectors of the original model. This example shows the modeling ability of the proposed method.

4.2. NACA 2415 airfoil structure problem

A NACA 2415 airfoil structure clamped at one end is considered. The structural FE model is illustrated in Fig. 8. Two ailerons are connected to the first substructure by a frictionless hinge. Because there are two ailerons (Ω_2 and Ω_3), two rigid body

Table 5
Number of master DOFs used and number of DOFs used in the original and reduced models for the wind-turbine rotor problem.

$N_m^{(1)}$	$N_m^{(2)}$	$N_m^{(3)}$	$N_m^{(4)}$	N_m	N_b	N_g	N_1
505	498	498	498	1999	288	94906	2287

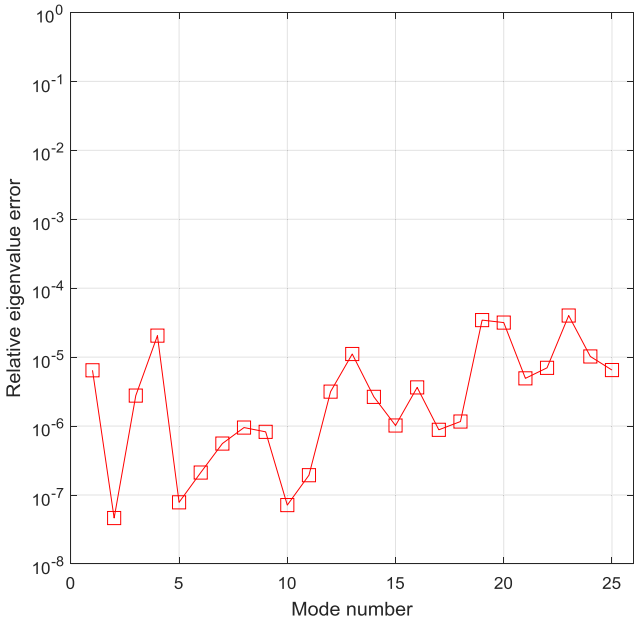

Fig. 12. Relative eigenvalue errors in the wind-turbine rotor problem.

Table 6
Computational costs for the wind-turbine rotor problem in Fig. 12.

Items	Computation times	
	[s]	Ratio [%]
Load system matrices ($\mathbf{M}^{(i)}$, $\mathbf{K}^{(i)}$,$\mathbf{B}^{(i)}$)	0.55	0.06
DOF decomposition (master & slave DOFs)	0.13	0.02
Substructural static pre-condensation	282.94	33.58
Substructural dynamic condensation	558.85	66.33
Assemble all the substructural reduced matrices	0.10	0.01
Total	842.57	100.00

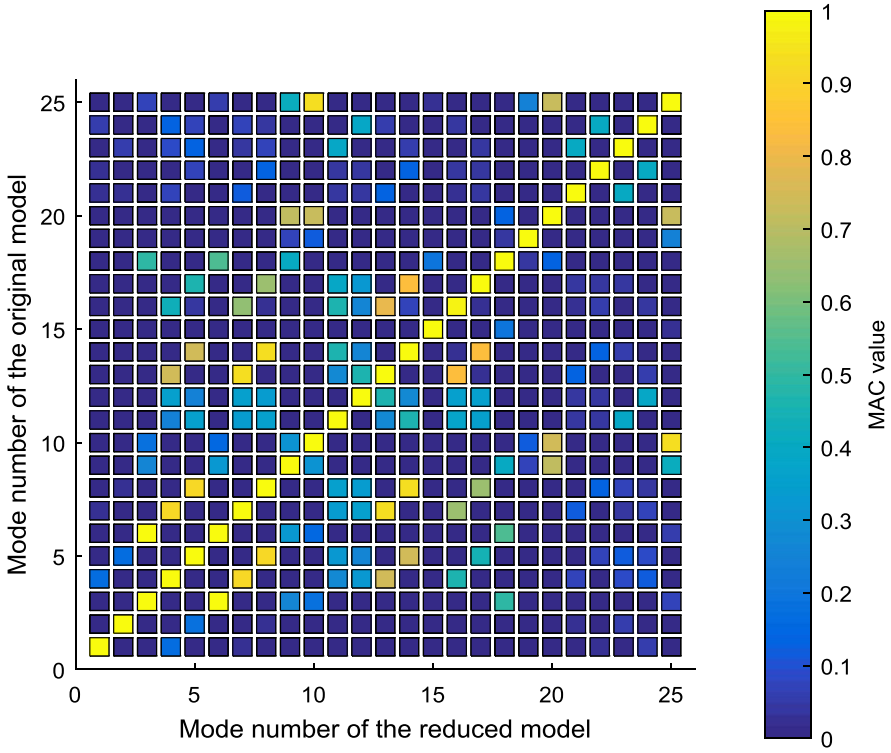

Fig. 13. MAC for the reduced model obtained using the proposed method in the wind-turbine rotor problem.

modes are calculated in the eigenvalue analysis of both global and reduced eigenvalue problems. The frictionless hinges between ailerons and airfoil are modeled using Lagrange multipliers.

Length L is 0.9144 m, width W is 0.2286 m, and thickness H is 0.0345 m. Young's modulus E is 71 GPa, Poisson's ratio v is 0.33, and density ρ is 3000 kg/m^3. The structure is an assemblage of three substructural FE models ($N_s = 3$). Each substructure is modeled using 3873 (Ω_1), 112 (Ω_2), and 144 (Ω_3) shell elements, respectively (19250, 725, and 925 DOFs).

Table 4 lists the number of master DOFs used and the number of DOFs used in the original and reduced models. The reduced model has a size of only 11% of the original model. Fig. 9 presents the relative eigenvalue errors obtained using the proposed method. Fig. 10 presents the MAC for the reduced model constructed using the proposed method. In this problem, the MAC of two rigid body modes are also considered. The results show the robustness of eigenpairs approximated by the proposed method, as in the previous examples.

4.3. Wind-turbine rotor problem

We consider a 600 kW wind-turbine rotor structure as shown in Fig. 11. The rotor diameter is 39.76 m, Young's modulus E is 58 GPa, Poisson's ratio v is 0.43, and density ρ is 1700 kg/m^3. The FE model and its mass and stiffness matrices were obtained using the commercial FE analysis software, ADINA [36–41].

The structure is an assemblage of four substructures ($N_s = 4$): a rotor hub and three turbine blades. The FE model of the rotor hub has 508 shell elements and 560 nodes, all the nodes are modeled by 5 DOFs. The FE model of each turbine blade has 5082 shell elements and 5101 nodes. Due to its shell-shell intersection on the blade edge, all nodes of the turbine blades are modeled by 6 DOFs. Table 5 lists the number of master DOFs used and the number of DOFs used in the original and reduced models.

In order to link the translational DOFs of the rotor hub and turbine blade FE models, Lagrange multipliers are adopted along their interfaces. In Guyan and IRS methods, such complicated assembly interfaces are hard to consider. For structures with repetitive patterns as in this numerical example, the proposed method is very efficient because it does not need to model all repeating substructures [24].

Fig. 12 presents the relative eigenvalue errors obtained by the proposed method, and Table 6 shows the detailed computational costs. Fig. 13 presents the MAC for the reduced model. Note that rigid body modes are not considered in this problem. The pairs of eigenvectors from the original and reduced models in each mode are shown with acceptable consistency.

5. Conclusions

In this study, we proposed a useful dynamic condensation method with free interface substructuring. Independently defined substructural FE models were individually reduced using the IRS method and the reduced substructural mass and stiffness matrices were assembled adopting Lagrange multipliers. As a result, we obtained two important advantages, the independence of substructural models and the ability to model complicated substructural interfaces. That is, the proposed method could handle relatively larger and more complex FE models than possible with the Guyan reduction and IRS methods. The detailed formulation was presented and the advantages were demonstrated through numerical examples.

In future work, it would be valuable to develop an optimized parallel computation algorithm using multi-processes for the proposed method to deal with FE models with a large number of substructures and DOFs. The method could then be used as an attractive solution for constructing accurate reduced models for experimental-FE model correlation, FE model updating, and optimizations.

Acknowledgement

This work was supported by the National Research Foundation of Korea (NRF) grant funded by the Korea government (MSIT) (No. NRF-2018R1A2B3005328). This work was also supported by "Human Resources Program in Energy Technology" of the Korea Institute of Energy Technology Evaluation and Planning (KETEP), granted financial resource from the Ministry of Trade, Industry & Energy, Republic of Korea (No. 20184030202000).

References

[1] R.J. Guyan, Reduction of stiffness and mass matrices, AIAA J. 3 (2) (1965) 380.
[2] J. O'Callahan, A procedure for an improved reduced system (IRS) model, in: Proceedings of the 7th International Modal Analysis Conference, Las Vegas, 1989, pp. 17–21.
[3] J. O'Callahan, P. Avitabile, R. Riemer, System equivalent reduction expansion process (SEREP), in: Proceedings of the 7th International Modal Analysis Conference, Las Vegas, 1989, pp. 29–37.
[4] M.A. Blair, T.S. Camino, J.M. Dickens, An iterative approach to a reduced mass matrix, in: 9th Conference International Modal Analysis Conference (IMAC), 1991, pp. 621–626.
[5] M.I. Friswell, S.D. Garvey, J.E.T. Penny, Model reduction using dynamic and iterated IRS techniques, J. Sound Vib. 186 (2) (1995) 311–323.
[6] T. Yin, H.F. Lam, H.M. Chow, H.P. Zhu, Dynamic reduction-based structural damage detection of transmission tower utilizing ambient vibration data, Eng. Struct. 31 (9) (2009).
[7] C.W. Kim, M. Kawatani, Pseudo-static approach for damage identification of bridges based on coupling vibration with a moving vehicle, Struct. Infrastruct. E 4 (5) (2008) 371–379.
[8] P. Mcgowan, A. Angelucci, M. Javeed, Dynamic test/analysis correlation using reduced analytical models, in: 33rd Structures Structural Dynamics and Materials Conference, 1992, p. 2335.
[9] P. Avitabile, Model reduction and model expansion and their applications–part 1 theory, Proceedings of the Twenty-Third International Modal Analysis Conference, 2005.
[10] W.C. Hurty, Dynamic analysis of structural systems using component modes, AIAA J. 3 (4) (1965) 678–685.
[11] R.R. Craig, A.J. Kurdila, Fundamentals of Structural Dynamics, John Wiley & Sons, 2006.
[12] R.R. Craig, M.C.C. Bampton, Coupling of substructures for dynamic analysis, AIAA J. 6 (7) (1968) 1313–1319.
[13] J.G. Kim, P.S. Lee, An enhanced Craig-Bampton method, Int. J. Numer. Methods Eng. 103 (2015) 79–93.
[14] J.G. Kim, S.H. Boo, P.S. Lee, An enhanced AMLS method and its performance, Comput. Methods Appl. Mech. Eng. 287 (2015) 90–111.
[15] S.H. Boo, J.G. Kim, P.S. Lee, A simplified error estimator for the CB method and its application to error control, Compt. Struct. 164 (2016) 53–62.
[16] S.H. Boo, J.G. Kim, P.S. Lee, Error estimation method for automated multi-level substructuring method, Int. J. Numer. Methods Eng. 106 (11) (2016) 927–950.
[17] J. Kim, S.H. Boo, P.S. Lee, Considering the higher-order effect of residual modes in the Craig-Bampton method, AIAA J. 56 (1) (2017) 403–412.
[18] S.H. Boo, J.H. Kim, P.S. Lee, Towards improving the enhanced Craig-Bampton method, Comput. Struct. 196 (2018) 63–75.
[19] K.C. Park, Y.H. Park, Partitioned component mode synthesis via a flexibility approach, AIAA J. 42 (6) (2004) 1236–1245.
[20] D. Markovic, A. Ibrahimbegovic, K.C. Park, Partitioning based reduced order modelling approach for transient analyses of large structures, Eng. Comput. 26 (1/2) (2009) 46–68.
[21] D.J. Rixen, A dual Craig-Bampton method for dynamic substructuring, J. Comput. Appl. Math. 168 (1–2) (2004) 383–391.
[22] D.J. Rixen, Dual Craig-Bampton with enrichment to avoid spurious modes, Proceedings of the IMAC-XXVII Conference & Exposition on Structural Dynamics, Orlando, USA, 2009.
[23] J.H. Kim, J. Kim, P.S. Lee, Improving the accuracy of the dual Craig-Bampton method, Compt. Struct. 191 (2017) 22–32.
[24] Akçay D Perdahcıoğlu et al, An optimization method for dynamics of structures with repetitive component patterns, Struct. Multidisc. Optim. 39 (6) (2009) 557–567.
[25] C. Brecher, M. Fey, C. Tenbrock, M. Daniels, Multipoint constraints for modeling of machine tool dynamics, J. Manuf. Sci. E-T ASME 138 (5) (2016) 051006.
[26] N. Bouhaddi, R. Fillod, Substructuring using a linearized dynamic condensation method, Compt. Struct. 45 (4) (1992) 679–683.
[27] N. Bouhaddi, R. Fillod, A method for selecting master DOF in dynamic substructuring using the Guyan condensation method, Compt. Struct. 45 (5–6) (1992) 941–946.
[28] H. Kim, M.H. Cho, Improvement of reduction method combined with sub-domain scheme in large-scale problem, Int. J. Numer. Methods Eng. 70 (2) (2007) 206–251.
[29] M. Cho, S. Baek, H. Kim, K.O. Kim, Identification of structural systems using an iterative, improved method for system reduction (TN), AIAA J. 47 (9) (2009) 2255.
[30] H. Kim, M.H. Cho, Sub-domain reduction method in non-matched interface problems, J. Mech. Sci. Technol. 22 (2) (2008) 203.
[31] H. Kim, M.H. Cho, H. Kim, H.G. Choi, Efficient construction of a reduced system in multi-domain system with free subdomains, Finite Elem. Anal. Des. 47 (9) (2011) 1025–1035.
[32] S.H. Boo, P.S. Lee, A dynamic condensation method using algebraic substructuring, Int. J. Numer. Methods Eng. 109 (12) (2017) 1701–1720.
[33] S.H. Boo, P.S. Lee, An iterative algebraic dynamic condensation method and its performance, Comput. Struct. 182 (2017) 419–429.
[34] R.D. Henshell, J.H. Ong, Automatic masters for eigenvalue economization, Earthq. Eng. Struct. D 3 (4) (1974) 375–383.
[35] J.H. Ong, Improved automatic masters for eigenvalue economization, Finite Elem. Anal. Des. 3 (2) (1987) 149–160.

[36] K.J. Bathe, Finite Element Procedure, Prentice Hall, 2006.
[37] K.J. Bathe, E.N. Dvorkin, A formulation of general shell elements - the use of mixed interpolation of tensorial components, Int. J. Numer. Methods Eng. 22 (3) (1986) 697–722.
[38] P.S. Lee, K.J. Bathe, Development of MITC isotropic triangular shell finite elements, Comput. Struct. 82 (11–12) (2004) 945–962.
[39] Y. Lee, P.S. Lee, K.J. Bathe, The MITC3+ shell finite element and its performance, Comput. Struct. 138 (2014) 12–23.
[40] Y. Lee, H.M. Jeon, P.S. Lee, K.J. Bathe, The modal behavior of the MITC3+ triangular shell element, Comput. Struct. 153 (2015) 148–164.
[41] ADINA system 9.3, ADINA R & D Inc., Watertown, MA; January 2017.
[42] M. Pastor, M. Binda, T. Harčarik, Modal assurance criterion, Proc. Eng. 48 (2012) 543–548.
[43] R.J. Allemang, The modal assurance criterion–twenty years of use and abuse, Sound Vib. 37 (8) (2003) 14–23.